A&A, 694, A251 (2025)
https://doi.org/10.1051/0004-6361/202452046

Astronomy & Astrophysics

Statistical investigation of solar flares showing quasi-periodicity based on STIX quick-look light curves

Ż. Szaforz[1,⋆], T. Mrozek[1,⋆], and M. Tomczak[2,⋆]

[1] Space Research Centre, Polish Academy of Sciences (CBK PAN), ul. Bartycka 18a, 00-716 Warszawa, Poland
[2] Astronomical Institute, University of Wrocław ul. Kopernika 11, 51-622 Wrocław, Poland

Received 29 August 2024 / Accepted 2 January 2025

ABSTRACT

Context. The emission of radiation associated with the release of energy in solar flares is often modulated according to a quasi-oscillatory pattern. This behavior is known as quasi-periodic pulsation (QPP). In this work, the STIX instrument on board Solar Orbiter was used to study solar flares that show quasi-periodic variations in X-ray emission.
Aims. This work aimed to conduct a statistical study of the periods and amplitudes of QPPs observed in quick-look light curves of the STIX instrument.
Methods. The quick-look light curves recorded from April 14, 2020 (the beginning of the mission) to the end of March, 2022 were scrutinized. 129 flares with the most distinct pulses were selected, for which the periodicity analysis was carried out using the Lomb-Scargle periodogram and the autocorrelation method. This sample contained mostly weak B- and C-class flares.
Results. It was found that 70% of examined flares showed statistically significant oscillations. Longer periods occur less frequently than shorter ones. We also identified a relationship between the period and the duration in which the oscillations were observed.

Key words. Sun: flares – Sun: oscillations

1. Introduction

The term quasi-periodic pulsations (QPPs) covers all periodic and quasi-periodic changes in the radiation emitted during flares. We often observe very characteristic fast and impulsive changes in the light curves of solar flares. Subsequent emission peaks can be recorded at quite regular time intervals, while the amplitudes of individual pulses usually change during the evolution of the phenomenon (Foullon et al. 2005; Nakariakov & Melnikov 2009; Nakariakov et al. 2010; Zaitsev et al. 2014). In some flares, QPPs are only visible in one particular phase, i.e in the impulsive or decay phase (Kane et al. 1983; Jakimiec & Tomczak 2012), in others – in all phases of the flare (Van Doorsselaere et al. 2011; Dolla et al. 2012; Kupriyanova & Ratcliffe 2016). In the case of QPPs observed in the decay phase, decaying quasi-harmonic oscillations are often visible (Kim et al. 2012; Nakariakov et al. 2019). In general, the QPP period remains constant throughout the observation period. However, there are observations of flares in which this period changes significantly with the evolution of the flare (Reznikova & Shibasaki 2011). Moreover, an increasing number of observations suggest that many flares exhibit several periods of QPPs simultaneously (Inglis & Nakariakov 2009; Tan et al. 2010; Tomczak & Szaforz 2014).

Quasi-periodic pulsations were recorded in flare-intensity profiles across the entire electromagnetic spectrum, from radio to the gamma range, and in nonthermal and thermal radiation. The largest number of observations were made in hard X-rays (HXRs) and in microwave radiation, where quasi-periodic changes are often very pronounced. The observed QPP periods range from fractions of seconds to several dozen minutes. It should be noted, however, that the temporal resolution of instruments limits this interval. On the other hand, solar flares are assumed to be phenomena that last only for a certain duration. This fact limits the possibility of detecting longer periods.

The mechanism causing QPPs is not yet clearly understood. Many theoretical models exist that have been described in a review paper by McLaughlin et al. (2018). Kupriyanova et al. (2019) also reviewed theoretical models of the QPPs' excitation, mentioning twelve models divided into the following three groups:

– Direct modulation of radiation emission caused by magneto-hydrodynamic (MHD) waves or electromagnetic oscillations of various types
– Modulation of the efficiency of the energy release process
– Spontaneous, quasi-periodic energy release

Not all aforesaid mechanisms included in these two reviews overlap. For example, McLaughlin et al. (2018) did not mention the flapping oscillation mechanism described by Kupriyanova et al. (2019). Unlike McLaughlin et al. (2018), the work of Kupriyanova et al. (2019) does not describe a model of wave packets with different dispersions. In another review, Zimovets et al. (2021), two additional models are considered: Kelvin-Helmholtz instability and current sheath thermal instability.

Starting with the first detections in the 1960s (Thompson & Maxwell 1962; Parks & Winckler 1969), quasi-periodic variations in solar flare radiation have become an object of interest for many scientists. Most research was conducted based on case studies. However, in recent years, attempts have been made to perform a statistical analysis of QPPs.

⋆ Corresponding authors; zs@cbk.pan.wroc.pl; tmrozek@cbk.pan.wroc.pl; michal.tomczak@uwr.edu.pl

Simões et al. (2015) analyzed 35 X-class flares observed during the 24th solar cycle with the X-ray Sensor (XRS; Chamberlin et al. 2009) onboard Geostationary Operational Environmental Satellites (GOES). Wavelet analysis was used to search for pulsations. QPPs were detected in approximately 80% of the events examined. Typical periods were in the range of 16–53 s. On the other hand, in Inglis et al. (2016), nearly 700 M- and X-class flares observed from 2011–2015 were studied. Observations were used from the GOES satellite in SXR and the Gamma-ray Burst Monitor (GBM) instrument onboard the *Fermi* Gamma-ray Space Telescope (Meegan et al. 2009) satellite in hard X-ray. The analysis was performed with the AFINO code described by Anfinogentov et al. (2022). This time, the presence of QPPs in the GOES data was confirmed in only 30% of examined flares. Moreover, only 8% of the same events showed QPPs in HXR. The determined periods were similar to those detected in Simões et al. (2015) and ranged between 10 and 30 s.

The work of Hayes et al. (2020) also used the AFINO code to search for QPPs in GOES data. For this study, they considered a total of 5519 flares of GOES C class and higher occurring between 2011 and 2018. The authors showed that approximately 46% of X-class flares, approximately 20% of M-class flares, and approximately 9% of C-class flares exhibited QPP signatures. The decrease in the detected number of flares with brightness class may be due to a reduced signal-to-noise ratio for fainter phenomena. Periods in the range of 6–300 s (predominately between 10–40 s ($\pm 1\sigma$)) were observed. It was found that there is no correlation between the QPPs period and the strength of the flare or the properties of the active region in which the flare occurred. However, a relationship was found between the period and the estimated parameters of the two-ribbon structure, such as ribbon separation, ribbon surface, and magnetic flux. The period was also correlated with the duration of the flare: longer flares showed QPPs with longer periods. It was also noticed that the oscillations observed in the decay phase of the flare were longer than those observed in the impulse phase.

A statistical analysis of QPPs in HXR was performed in Szaforz & Tomczak (2019) for 74 behind-the-limb flares observed with the HXT instrument onboard the *Yohkoh* satellite. However, periodicity was only derived in light curves with a sufficiently high signal-to-noise ratio. It was shown that in 14–23, 23–33, and 33–55 keV energy ranges, approximately 35% of the observed flares had QPPs. In the 53–93 keV energy range, this result was much higher (67%). However, in this channel, a sufficiently high signal-to-noise ratio was observed for only six flares, which makes the statistical analysis unreliable. We can therefore say that the obtained statistics of flares associated with QPPs are consistent with the results of Inglis et al. (2016) and Hayes et al. (2020). The observed periods ranged widely from 20 to 317 s.

In this work, we searched for QPPs in the data collected by the Spectrometer Telescope for Imaging X-rays (STIX; Krucker et al. 2020). In Sect. 2, we briefly describe observational data, Sect. 3 contains a description of the methodology used to determine periodicity, while in Sect. 4 the results of the statistical analysis are presented. Section 5 contains a short summary of the results of this work.

2. Observations

Solar Orbiter (Müller et al. 2020) is a space probe built by ESA in cooperation with NASA, launched on February 10, 2020. It orbits the Sun with varying distances and inclinations. The minimum distance between Solar Orbiter and the Sun reaches 0.28 a.u. at perihelion. Ten scientific instruments including STIX are onboard. The STIX provides spectroscopic data in the range of 4–150 keV, with a spectral resolution as high as 1 keV at 6 keV and a time resolution down to 0.1 s. Since the Solar Orbiter launch, STIX collected scientific data for several weeks in 2020. Since 1 January 2021, STIX data have been recorded almost continuously. However, not all science data are downloaded due to telemetry limitations.

One of the STIX's quick-look data products is light curves. Although these data products' spectral and temporal resolution is limited, their great advantage is that they are downloaded continuously. Quick-look light curves are provided in five energy bands: 4–10, 10–15, 15–25, 25–50, and 50–84 keV with a time resolution of 4 s.

This work includes a review of the STIX instrument's quick-look light curves recorded from the mission's beginning (April 14, 2020) to the end of March, 2022. The STIX database catalogued 8409 flares during this period. Those were mostly weak flares. The distribution of GOES classes, estimated taking into account the number of STIX counts and the distance from the Sun (Xiao et al. 2023), is shown in Fig. 1a. We looked for flares with at least three distinctively observed radiation pulses (see Sect. 3). Due to the incomplete understanding of the impact of attenuators on the recorded flare flux, the phenomena during which the attenuator motion was triggered were omitted. Over 330 flares meeting the above conditions were found, 129 of which with either the strongest, most regular or long pulsations were analyzed. Estimated GOES classes for this group of flares ranged from B4.0 to X1.0. The distribution of the classes in the sample is presented in Fig. 1b.

3. Periodicity determination

Intuitively, we define QPPs in flares as a sequence of successive emission maxima characterized by similar visually temporal spacing. However, observations showed a large diversity of QPPs. In the observational data, QPPs are often difficult to recognize and parameterize. This is influenced by many factors, including the following:

- Different shapes of a slowly changing flare emission component (a trend).
- Visible changes in the period and amplitude of QPPs during the flare.
- Pulsation damping.
- Anharmonic shape of individual pulses.
- Superposition with noise.
- Low quality of QPPs observations.

Broomhall et al. (2019) tested eight different methods for detecting QPPs with varying properties in simulated and observed flare light curves. In the tests, they considered the effects of detrending and data trimming, the effects of noise, non-stationarity, and the period drift of QPPs. The detection techniques used in Broomhall et al. (2019) include both traditionally used methods (Fourier periodogram, wavelet analysis) and new generation methods, increasingly used in the study of solar observations, such as empirical mode decomposition (EMD) and Bayesian analysis.

The test showed that no method works perfectly for every type of observation. For example, the Fourier periodogram effectively detects high-quality harmonic oscillations with stable period(s) in noisy time series. To search for QPPs with a non-stationary or slowly drifting period, wavelet analysis is more suitable. The EMD method is preferred for analyzing complex

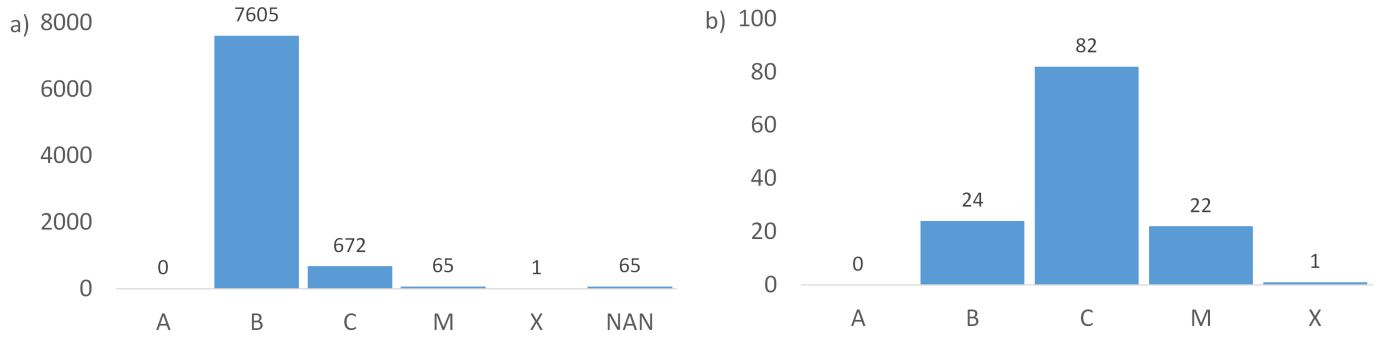

Fig. 1. Estimated GOES classes for solar flares in the STIX catalogue. Panel (a) shows the distribution of estimated GOES classes for all flares observed between April 14, 2020, and March 31, 2022, including events without automatic class estimation (labeled as NAN). Panel (b) focuses on the subset of 129 selected flares, highlighting their distribution across the estimated classes.

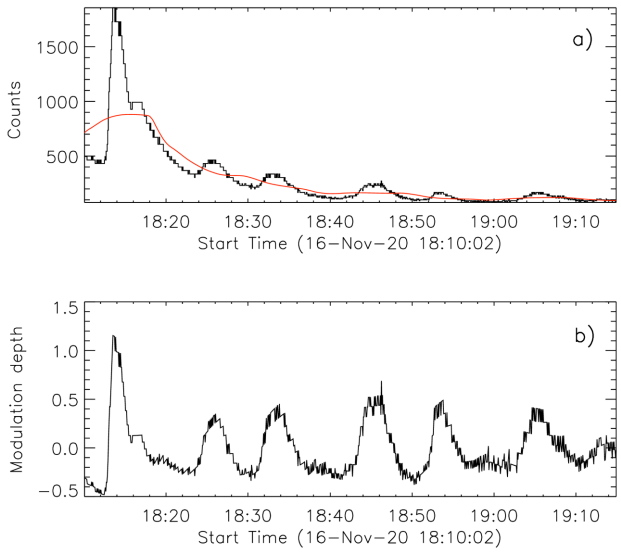

Fig. 2. Temporal analysis of the November 16, 2020 flare observed by STIX. (a) Flux recorded in the 4–10 keV channel, with the red line indicating the running average fit. (b) Normalized time series $S(t)$.

time series with an anharmonic form or a strongly nonstationary period. Bayesian methods allow for robust estimates of QPP parameters and their uncertainties, provided that the model function is properly specified. The application of several independent techniques has proven beneficial to improving the reliability of QPPs detection.

In HXRs, QPPs typically superimpose a standard light-curve profile (Gryciuk et al. 2017), which shows a rapid rise followed by a gradual decline. Broomhall et al. (2019) showed that trend subtraction can positively impact the pulsation detection process, but only if done with due care by individually selecting parameters for each time series. Automating the trend subtraction process often leads to a relatively high number of false pulsation detections.

In this work, we subtracted the trend and created a normalized time series $S(t)$:

$$S(t) = \frac{F(t) - \hat{F}(t)}{\hat{F}(t)}, \tag{1}$$

where $F(t)$ is the observed HXR radiation flux and $\hat{F}(t)$ is the running average of $F(t)$. The window width used to calculate the running average was selected individually for each light curve so that no artificial pulses were created during the subtraction process. Both the duration of the flare and the period of the identified pulsations were taken into account. The window widths selected for the analyzed flares are included in Table A.1. An example of the STIX light curve with a fit average for the November 16, 2020 flare is shown in Fig. 2, panel a). For this flare, the width of the smoothing window was 600 s. Panel b) of this figure shows the normalized time series $S(t)$.

The QPP periods were determined using two independent methods. The first applied technique is the Lomb-Scargle periodogram (Lomb 1976; Scargle 1982; VanderPlas 2018). This is a method based on the Fourier transform (Auchère et al. 2016), whose greatest advantage over other methods for determining periodicity is that it can be used in the case of unevenly sampled time series. A good metric to express the significance of a period designated by a Lomb-Scargle periodogram is false alarm probability (FAP). A false positive occurs in periodic analysis techniques when a period is mistakenly detected when there is none. The lower the FAP value for a given period P, the more likely it is that it is a significant period. FAP values are expressed as numbers ranging from zero to one. In this work, the level of FAP = 0.01 was used as the criterion for the significance of the periods obtained in the Lomb-Scargle periodograms.

The Lomb-Scargle periodogram calculated for the flare of November 16, 2020 is presented in the upper panel of Fig. 3. The dashed line corresponds to the significance level of the FAP method = 0.01. We can identify several peaks above the level. The highest of them corresponds to the period 611 s. The subsequent maxima correspond to periods of approximately 380 and 1050 s: that is, half and twice the main period, respectively. The first of these periods corresponds to the frequency of the second harmonic of the observed signal. These types of maxima appear quite often in periodograms.

The second method for quantifying quasi-periodic pulsation, the autocorrelation function, was used to verify the results obtained using the Lomb-Scargle periodogram. It examines the relationship between successive points in a time series and provides information about randomness in the data set. If the set is random, the autocorrelation should be below the confidence level, regardless of the time offset used between the data. For the significance level of 0.05, the values of the autocorrelation function calculated for white Gaussian noise are within $\pm 1.96 N^{-1/2}$ (N is the number of elements in the data set). If above the significance level, the position of the maximum of the autocorrelation function for the nonzero argument determines the period of the signal in the time series (Chatfield 2004; Brockwell & Davis 2016). The autocorrelation method can only be used for uni-

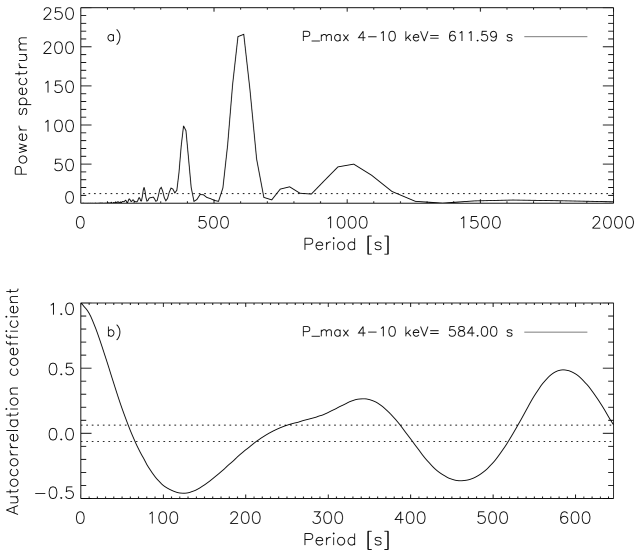

Fig. 3. Analysis of periodicity for the November 16, 2020 flare. (a) Power spectrum calculated using Lomb-Scargle method, with the dashed line corresponding to the significance level of the FAP method = 0.01. (b) Autocorrelation coefficient function for the same flare, where the dashed lines represent a significance level of 0.05.

formly sampled time series. If this condition is not met, the time series must be interpolated before applying it. However, there was no need for interpolation in the case of the STIX quick-look light curves, as they are uniformly sampled. This method also gives incorrect results for long periods compared to the entire time series given to the analysis. The analysis assumed that this method works correctly for periods shorter than 1/6 of the length of the tested time series. It is worth noting that in such cases the designated period often corresponds to the frequency of the second harmonic of the real signal: that is, it is half as long as the real one.

The autocorrelation function for the example flare is shown in Fig. 3b. Here, we see a stronger maximum for the period of 584 s, which is similar to that obtained from the Lomb-Scargle method. The second maximum of the function corresponds to a period of 342 s.

In this work, the following criteria were taken into account to determine whether we are dealing with QPPs during a solar flare:

1. At least three pulses are visible in the normalized time series.
2. The maximum in the Lomb-Scargle periodogram is significant at the FAP level = 0.01.
3. The maximum of the autocorrelation function is above the significance level of 0.05.
4. The difference between the period obtained by the autocorrelation function and the period obtained from Lomb-Scargle method is less than 15% of the longer period of those two. Since each method can show several maxima above its corresponding level of significance, a maximum of the three strongest maxima were taken into account for each method.

Of the sample of 129 flares analyzed, 91 met the first two criteria for at least one energy interval. 62 flares met all requirements.

The values of the periods corresponding to the strongest maximum in the Lomb-Scargle periodogram and the autocorrelation function are included in Table A.1. If several maxima were observed and the value of the weaker period was consistent with the period determined by the second method or in another energy channel of a given flare, this value was also included in Table A.1. Index (1) indicates situations when the period determined by the Lomb-Scargle method was outside the range of the autocorrelation method. Sometimes it happened that one of the methods gave periodicity on the border of the significance level, but the obtained value was consistent with the periodicities determined by the second method or in other energy channels of the examined flare. These periods are also placed in Table A.1 and marked with index (2).

4. Statistical analyses

In Fig. 4, the flares examined in this paper are divided into five groups defined by the following criteria:

- The strongest maxima present in the Lomb-Scargle periodogram and in the autocorrelation function indicated the same oscillation period with the difference less than 15% of the longer period.
- In case any of the methods showed more than one maximum above its significance level, we considered a maximum of the three strongest maxima. If in any case the difference between the maximum present in the Lomb-Scargle periodogram and the maximum indicated by the autocorrelation function was less than 15% of the longer of those two periods, the flare fell into this group.
- The strongest maximum determined by the Lomb-Scargle method was outside the range of the autocorrelation method.
- Both methods showed maxima with clearly different periods.
- Both methods gave results below the appropriate significance levels; therefore, no periodicity was detected.

The top panel of Fig. 4 shows a summary graph considering observations in all energy channels. If oscillations were observed in several channels, the one for which the highest maximum in the Lomb-Scargle periodogram was obtained was considered. This graph shows that statistically significant periodicity was observed in 70% of the examined solar flares. In the case of 62 events, the period determined by the Lomb-Scargle method was confirmed by the autocorrelation method. The subsequent plots in this figure were created for the periodicities observed in the light curves in individual STIX energy channels. No graphs are shown for the channels 25–50 and 50–84 keV, because in these cases only three and two analyzed cases showed a statistically significant periodicity, respectively.

Significant periodicity was therefore observed in 54, 59, and 43 flares, examined in channels 4–10, 10–15, and 15–25 keV, respectively. It should be noted, however, that we only considered the analysis of flares for which the presence of several maxima in the light curves had previously been visually detected. On the other hand, if we consider all 8409 flares that took place during the period under study (from the beginning of the mission to the end of March 2022), the periodicities were observed in 32% of M-class flares, 9% of C-class flares, and 0.3% of B-class flares. The results are therefore consistent with the previous works of Simões et al. (2015) and Hayes et al. (2020). However, our sample is dominated by weak flares, which were not considered in previous analyses due to their low signal-to-noise ratios. Only a single case of X-class flare observed in the analyzed time period did not show QPP signatures. However, this is not enough to allow us to draw conclusions concerning the QPP statistics in X-class flares.

As shown in Hayes et al. (2020), longer periods are relatively less common. This is confirmed by the histograms shown in Fig. 5, where we see a decrease in the number of observations of longer periodicities in each energy channel. However,

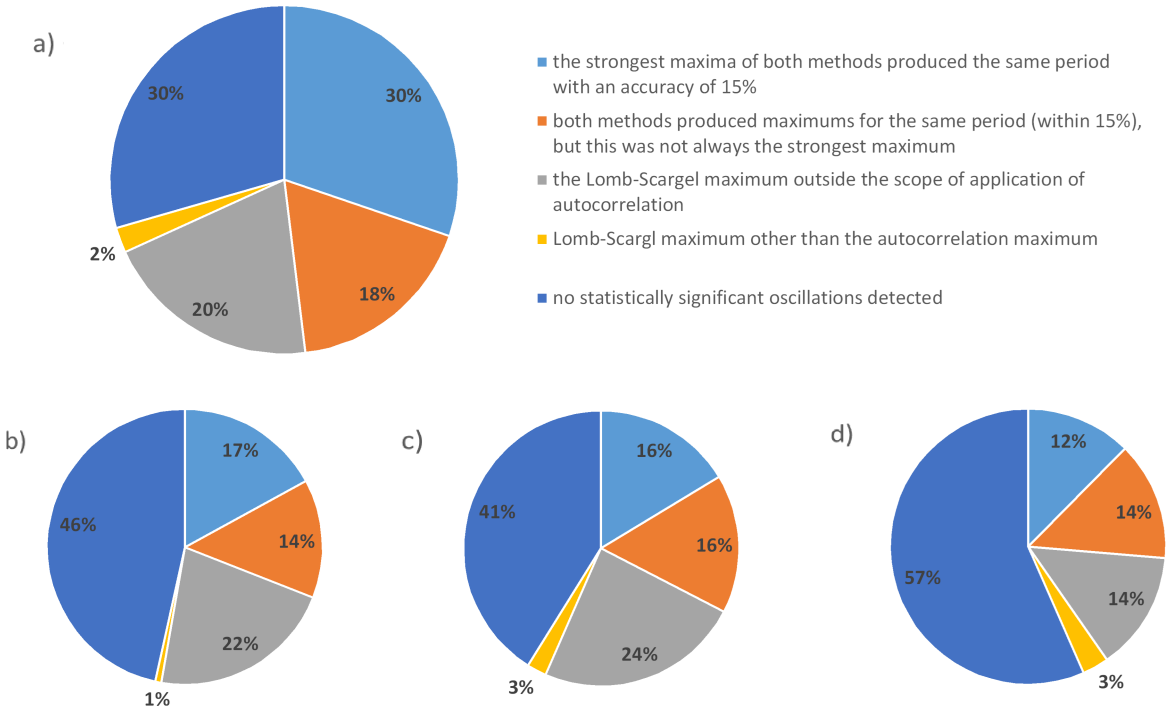

Fig. 4. Presence of statistically significant periodicities in light curves of 129 flares analyzed for periodicity. Panel (a) shows results for a statistically significant period in at least one energy channel. Panels (b), (c), and (d) show individual results for the periods observed in the 4–10 keV, 10–15 keV, and 15–25 keV channels, respectively.

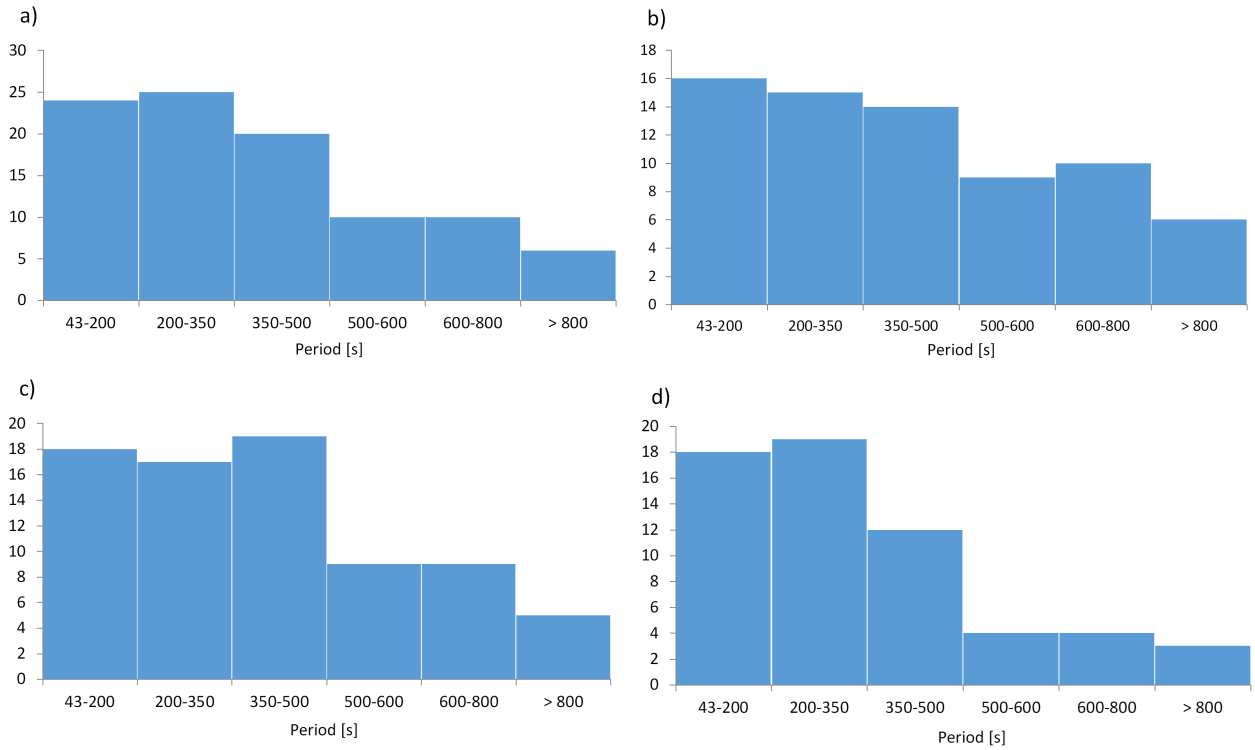

Fig. 5. Histograms of strongest periodicities visible in Lomb-Scargle periodograms. Only periodicities exceeding the significance level FIP = 0.01 were taken into account. In the case of four flares for which different averaging times or time intervals were used, two periodicities were obtained; both are included in the histogram. In panel (a), the strongest periodicity for each flare corresponds to the highest peak in the Lomb-Scargle periodogram, regardless of the energy channel. Panels (b), (c), and (d) correspond to the energy channel 4–10, 10–15, and 15–25 keV, respectively. The histograms include 95, 70, 77, and 58 flares, respectively.

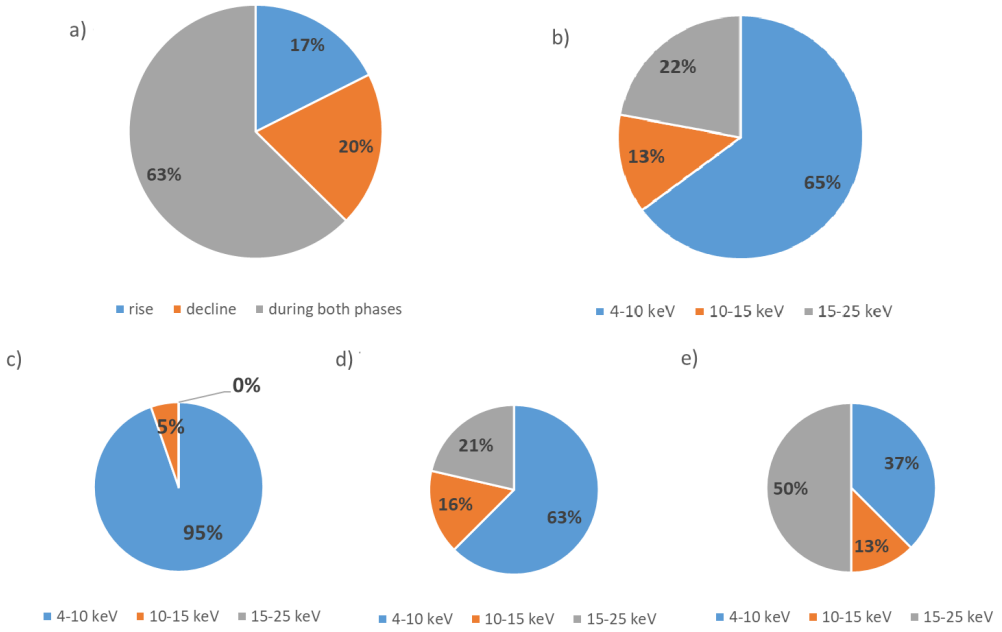

Fig. 6. Analysis of the occurrence and energy characteristics of quasi-periodic pulsations (QPPs) in solar flares. (a) Phases of the flare in which QPPs were detected. The analysis was performed for 91 flares for which the Lomb-Scargle method revealed statistically significant periodicities in the periodogram. (b) Energy range in which the detected periodicities were strongest, based on the same 91 flares where statistically significant periodicities were identified. Panels (c), (d), and (e) show results divided by estimated GOES class for 19 B-class flares, 56 C-class flares, and 16 M-class flares, respectively.

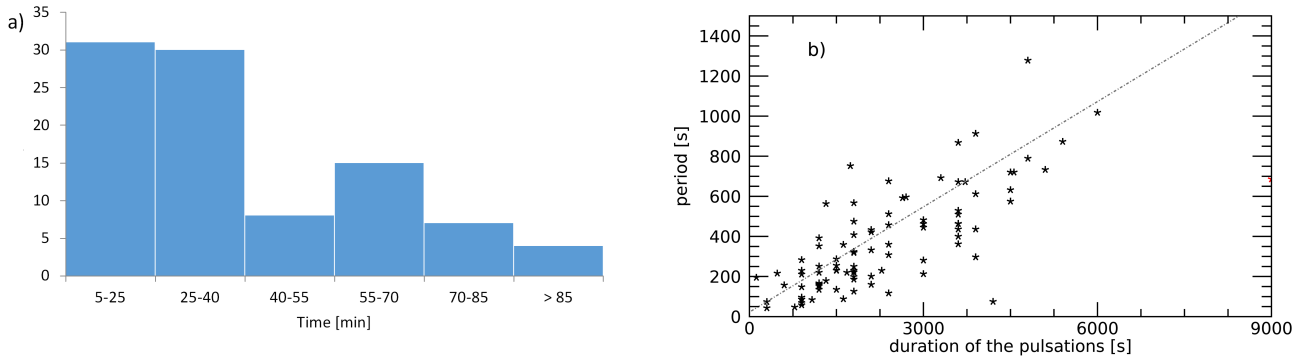

Fig. 7. Analysis of the characteristics of pulsations in solar flares. (a) Histogram of pulsation durations. (b) Relationship between pulsation duration and pulsation period. For each flare, the period with the strongest maximum in the Lomb-Scargle periodograms among all channels was assumed. The relationship is expressed as duration = 0.18*period + 22.53. The Pearson and Spearman correlation coefficients, calculated without two flares with the longest durations, are 0.76 and 0.73, respectively.

the majority of the periods observed by Hayes et al. (2020) lie in the 10–40 s range. The shortest period of oscillation determined in this work is 43 s. One possible reason why we did not observe shorter oscillations may be related to the time resolution of the data used. Due to data availability, the analysis here was performed for quick-look data with a resolution of 4 s – four times longer than the time resolution of GOES data used in Hayes et al. (2020). Since the end of January 2022, STIX has also continuously transmitted Spectrogram data to Earth with a resolution of up to 0.1 s. In future, such high time cadence will allow for an in-depth analysis of shorter periodicities.

As shown in Fig. 6a, the tested sample of flares included both phenomena in which QPPs were observed only in the rise and decay phase of the flare. However, the vast majority showed QPP signatures throughout the duration of the flare (63%). The strongest maximum in Lomb-Scargle periodograms was most often observed in the 4–10 keV energy channel (Fig. 6b). We can conclude that strong pulsations were more often observed in thermal emission, which dominates this energy channel, than in nonthermal emission, which is dominant in higher energy channels. However, when we analyze this dependence for flares of each estimated GOES class separately (Figs. 6c-d), we can clearly see that the higher the class, the more often we observe the strongest maximum at higher energies. This is in agreement with the fact that the stronger solar flares exhibit a higher proportion of hard X-ray emissions, highlighting the role of accelerated electrons in more energetic flares (Fletcher et al. 2011). The results in panel Fig. 6b are therefore due to the predominance of weak flares.

The histogram of the pulsation duration is shown in Fig. 7a. Next, in Fig. 7b, the relationship between the pulsation duration and the observed pulsation period is shown. The period

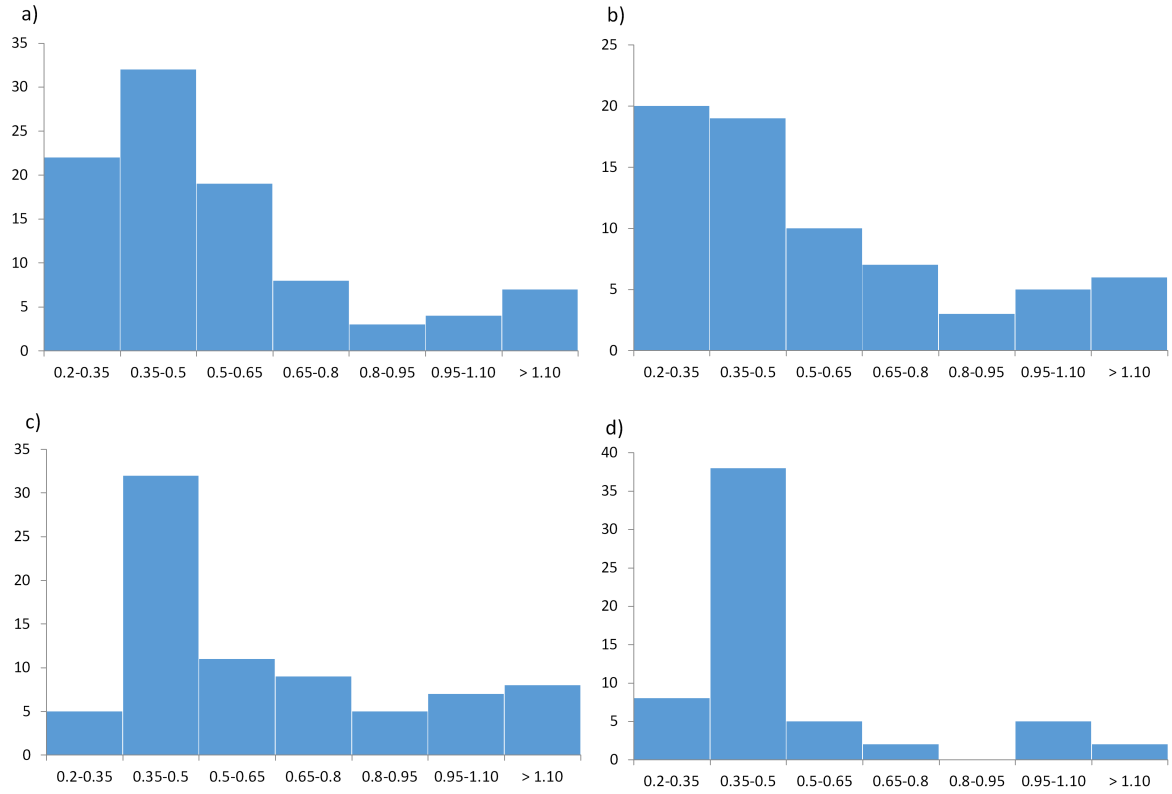

Fig. 8. Histograms of values of normalized amplitudes of light-curve modulations induced by QPPs. Panel (a) contains the highest amplitude observed for a given flare. Panels (b), (c), and (d) show the values observed in the 4–10, 10–15, and 15–25 keV channels, respectively.

that produced the strongest maximum in the Lomb-Scargle periodograms obtained for a given flare in all energy channels was adopted for each flare. Two flares were not included in the plot. These were the flares with the longest durations, whose relatively low pulsation periods make them stand out from the others. This suggests that a different mechanism for either the excitation or sustainment of pulsations could have been at work for them. The fact that in both of these events the signal between individual pulses drops almost to background level allows us to assume that we may even be dealing with a series of homologous flares. The Pearson and Spearman correlation coefficients, calculated without these two flares, are 0.76 and 0.73, respectively. This correlation is very similar to that found by Hayes et al. (2020) between the period and duration of the flare (Pearson's correlation coefficient is 0.67 and Spearman's is 0.71). Hayes et al. (2020) concluded that this correlation is not due to observational effects or limitations of the detection method used. This result means that oscillations with longer periods can propagate longer in the corona. In future, this relationship could be used to test theoretical models of QPPs. Unfortunately, at present the models do not predict such a relationship.

Histograms of the amplitude values of the normalized time series, obtained after subtracting the trend from the STIX light curves according to formula (1), are shown in Fig. 8. Typically, the highest amplitude values obtained for a given time series were taken into account here. In a few cases, the procedure of trend subtraction was not able to correctly separate the maximum from the trend. This led to an identified maximum significantly outweighing the others, and hence this maximum was omitted to reflect the behavior of the entire phenomenon. In the figures, we see the dominance of amplitudes in the range of 0.35–0.5, especially in the higher energy channels.

Figure 9a presents the behavior of the normalized amplitudes of the analyzed flares. We can see that most amplitudes had a chaotic, variable nature. A decrease in amplitude over time was observed for 17% of flares. The amplitude increased only in one case – the 16 November 2020 flare – at around 8:00 UT. It was a flare in which oscillations were visible in the rise phase. The period of these oscillations was 250 s.

For the examined flares, a weak relationship between the amplitude and the oscillation period was observed. Indeed, the longest periods were observed in cases where individual pulses were practically separated, so the amplitudes of these oscillations, even after normalization, were very large. The Pearson coefficient of the observed correlation is 0.56, and the Spearman coefficient is 0.40 (Fig. 9b).

5. Conclusions

This paper presents the results of the analysis of solar flares observed with the STIX instrument onboard Solar Orbiter. STIX offers new opportunities to study phenomena occurring on the Sun. One of the great advantages of STIX, in the context of this work, is the lack of modulated orbital background, which is an issue for experiments conducted on low Earth orbits. This is a significant simplification for time-series analysis. In addition, STIX has been continuously conducting observations since January 1, 2021.

The advantages of STIX were used to study quasi-periodic pulsations observed in solar flares. QPPs are one of the key properties of flares that can reveal information about energy-release processes and their impact on the Sun and the space environment. So far, a lot of work has been devoted to the study of QPPs. The majority of them determine the QPP characteristics of

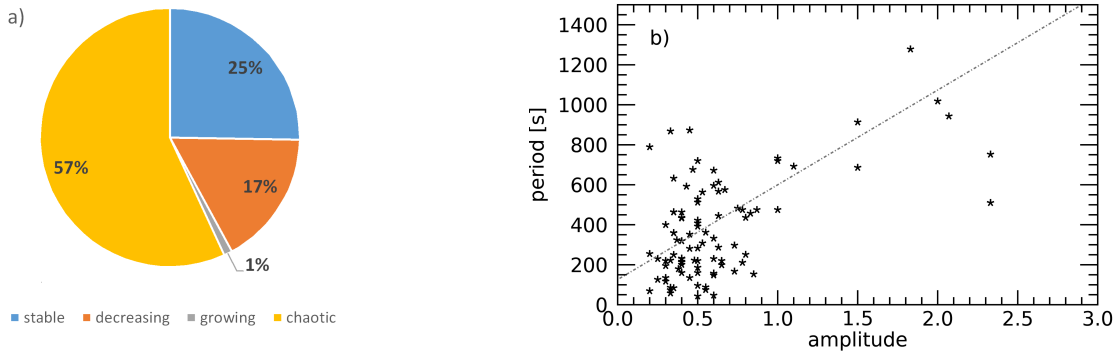

Fig. 9. Analysis of the amplitudes' behavior and their correlation with the pulsation period in solar flares. (a) Behavior of values of normalized amplitudes during flare. (b) Relationship between amplitude of normalized time series and pulsation period. The period with the strongest maximum in the Lomb-Scargle periodograms among all channels was assumed for each flare. The relationship is expressed as duration = 473.865*period + 125.955. The Pearson correlation coefficient is 0.56, and the Spearman correlation coefficient is 0.40.

selected flares, with the aim of referring to the theoretical model indicated by the author. In this work, we focused on statistical studies, which allowed us to obtain more representative results and identifying trends and relationships.

The STIX quick-look light curves recorded from April 14, 2020 (the beginning of the mission) to the end of March, 2022 were reviewed. We searched for flares with at least three radiation pulses that occur at visually equal intervals. 129 flares with the clearest pulses were selected, for which the feasibility of modulating the light curves was checked using two methods. The Lomb-Scargle method showed that 70% of the examined flares showed statistically significant oscillations. In the case of 48% flares, the autocorrelation method confirmed the presence of these periodicities. It has to be noted, however, that the periods determined by the first method for 20% of flares were beyond the scope of applicability of the second method. Taking into account all the 8409 cataloged flares during the investigation period, periodicities were observed in 32% of estimated GOES M-class flares, 9% of C-class flares, and 0.3% of B-class flares.

Statistical studies of the behavior of the determined oscillation periods and amplitudes were conducted. The observed periods were in the range of 43–1355 s. It was found that longer periods occur less frequently than shorter ones. It was also shown that there is a relationship between the period and the length of the time interval during which the oscillations were observed. Due to the fact that our sample was dominated by weak flares, pulsations were much more often observed in thermal emission, which dominates the 4–10 keV energy channel.

A continuation of this work is planned in the future. We intend to take a more detailed look at individual flares exhibiting QPPs in order to indicate the mechanism responsible for their excitation.

Acknowledgements. We would like to thank the anonymous reviewers for very helpful comments that significantly improved the article. We are also thankful to Arun Kumar Awasthi for language corrections and constructive comments and remarks. Solar Orbiter is a space mission of international collaboration between ESA and NASA, operated by ESA. The STIX instrument is an international collaboration between Switzerland, Poland, France, Czech Republic, Germany, Austria, Ireland, and Italy. This work was supported by the National Science Centre, Poland grant No. 2020/39/B/ST9/01591.

References

Anfinogentov, S. A., Antolin, P., Inglis, A. R., et al. 2022, Space Sci. Rev., 218, 9
Auchère, F., Froment, C., Bocchialini, K., Buchlin, E., & Solomon, J. 2016, ApJ, 825, 110
Brockwell, P. J., & Davis, R. A. 2016, Introduction to Time Series and Forecasting, Springer Texts in Statistics (Springer International Publishing)
Broomhall, A.-M., Davenport, J. R. A., Hayes, L. A., et al. 2019, ApJS, 244, 44
Chamberlin, P. C., Woods, T. N., Eparvier, F. G., & Jones, A. R. 2009, in Solar Physics and Space Weather Instrumentation III, eds. S. Fineschi, & J. A. Fennelly, SPIE Conf. Ser., 7438, 743802
Chatfield, C. 2004, The Analysis of Time Series: an Introduction, 6th edn. (Florida, US: CRC Press)
Dolla, L., Marqué, C., Seaton, D. B., et al. 2012, ApJ, 749, L16
Fletcher, L., Dennis, B. R., Hudson, H. S., et al. 2011, Space Sci. Rev., 159, 19
Foullon, C., Verwichte, E., Nakariakov, V. M., & Fletcher, L. 2005, A&A, 440, L59
Gryciuk, M., Siarkowski, M., Sylwester, J., et al. 2017, Sol. Phys., 292, 77
Hayes, L. A., Inglis, A. R., Christe, S., Dennis, B., & Gallagher, P. T. 2020, ApJ, 895, 50
Inglis, A. R., & Nakariakov, V. M. 2009, A&A, 493, 259
Inglis, A. R., Ireland, J., Dennis, B. R., Hayes, L., & Gallagher, P. 2016, ApJ, 833, 284
Jakimiec, J., & Tomczak, M. 2012, Sol. Phys., 278, 393
Kane, S. R., Kai, K., Kosugi, T., et al. 1983, ApJ, 271, 376
Kim, S., Nakariakov, V. M., & Shibasaki, K. 2012, ApJ, 756, L36
Krucker, S., Hurford, G. J., & Grimm, O. 2020, A&A, 642, A15
Kupriyanova, E. G., & Ratcliffe, H. 2016, Adv. Space Res., 57, 1456
Kupriyanova, E. G., Kashapova, L. K., Van Doorsselaere, T., et al. 2019, MNRAS, 483, 5499
Lomb, N. R. 1976, Ap&SS, 39, 447
McLaughlin, J. A., Nakariakov, V. M., Dominique, M., Jelínek, P., & Takasao, S. 2018, Space Sci. Rev., 214, 45
Meegan, C., Lichti, G., Bhat, P. N., et al. 2009, ApJ, 702, 791
Müller, D., St. Cyr, O. C., & Zouganelis, I. 2020, A&A, 642, A1
Nakariakov, V. M., & Melnikov, V. F. 2009, Space Sci. Rev., 149, 119
Nakariakov, V. M., Inglis, A. R., Zimovets, I. V., et al. 2010, Plasma Phys. Controlled Fusion, 52, 124009
Nakariakov, V. M., Kolotkov, D. Y., Kupriyanova, E. G., et al. 2019, Plasma Phys. Controlled Fusion, 61, 014024
Parks, G. K., & Winckler, J. R. 1969, ApJ, 155, L117
Reznikova, V. E., & Shibasaki, K. 2011, A&A, 525, A112
Scargle, J. D. 1982, ApJ, 263, 835
Simões, P. J. A., Hudson, H. S., & Fletcher, L. 2015, Sol. Phys., 290, 3625
Szaforz, Ż., & Tomczak, M. 2019, Adv. Space Res., 64, 1100
Tan, B., Zhang, Y., Tan, C., & Liu, Y. 2010, ApJ, 723, 25
Thompson, A. R., & Maxwell, A. 1962, ApJ, 136, 546
Tomczak, M., & Szaforz, Ż. 2014, Cent. Eur. Astrophys. Bull., 38, 111
VanderPlas, J. T. 2018, ApJS, 236, 16
Van Doorsselaere, T., De Groof, A., Zender, J., Berghmans, D., & Goossens, M. 2011, ApJ, 740, 90
Xiao, H., Maloney, S., Krucker, S., et al. 2023, A&A, 673, A142
Zaitsev, V. V., Stepanov, A. V., & Kaufmann, P. 2014, Sol. Phys., 289, 3017
Zimovets, I. V., McLaughlin, J. A., Srivastava, A. K., et al. 2021, Space Sci. Rev., 217, 66

Appendix A: QPP parameters collected for analyzed flares

Table A.1. Flares for which the Lomb-Scargle method detected statistically significant periodicity in at least one energy channel.

No.	Date	Duration of pulsations	Smoothing window width [s]	Period of Lomb-Scargle preiodogram [s]					Period of autocorrelation method [s]				
				4-10 keV	10-15 keV	15-25 keV	25-50 keV	50-84 keV	4-10 keV	10-15 keV	15-25 keV	25-50 keV	50-84 keV
1.	16.11.2020	04:58-05:20	200	179	179	179	-	-	166	82;180	102 [2]	-	-
2.	16.11.2020	07:45-08:15	200	250	250	-	-	-	232	232	-	-	-
3.	16.11.2020	18:10-19:15	600	612	590	386	-	-	584	580	348 [2]	-	-
4.	17.11.2020	07:50-08:40	600	445	428	463	-	-	222;406 [2]	214;404	214 [2]	-	-
5.	19.11.2020	00:00-00:30	600	475	475	475	-	-	228 [1]	228 [1]	226 [1]	-	-
6.	21.11.2020	04:50-05:40	600	463	463	399	-	-	496	490	240 [2];405 [2]	-	-
7.	05.03.2021	08:10-09:10	600	463	463	-	-	-	444	266 [2];452 [2]	-	-	-
8.	18.03.2021	14:49-15:02	60	47	-	-	-	-	45 [2];92	-	-	-	-
9a.	17.04.2021	16:00-17:00	600	-	-	529	-	-	-	-	290;520 [2]	-	-
9b.	17.04.2021	16:00-16:38	240	-	217	230	-	-	-	94,220	104,204	-	-
10.	22.04.2021	04:10-05:30	600	789	738	-	-	-	422 [1]	434 [1,2]	-	-	-
11.	02.05.2021	11:15-11:40	160	-	135	131 [2]	-	-	-	198 [2]	190 [2]	-	-
12.	05.05.2021	22:20-22:40	160	220	220	-	-	-	94 [1]	84 [1,2]	-	-	-
13.	07.05.2021	18:45-19:15	200	-	-	186	-	-	-	-	86;176 [2]	-	-
14.	09.05.2021	13:50-13:55	120	-	-	43 [2]	-	-	-	-	46	-	-
15.	18.05.2021	02:00-02:15	60	64 [2]	64 [2]	58 [2]	-	-	62 [2]	60	58	-	-
16.	21.05.2021	19:22-19:30	200	-	-	216	-	-	-	-	56 [1,2]	-	-
17.	22.05.2021	21:30-22:50	1200	1278	1355	1355	-	-	678 [1]	660 [1]	702 [1,2]	-	-
18.	23.06.2021	06:46-07:30	600	592	562;438	458	-	-	316;580 [1]	258 [1]	446	-	-
19.	28.06.2021	19:06-19:11	60	74	74	52 [2]	-	-	40 [1]	36 [1,2]	26 [1]	-	-
20.	13.07.2021	17:55-18:45	200	-	399	213	-	-	-	218;410	210;426	-	-
21.	15.07.2021	21:05-21:30	200	-	-	255	255	255	-	-	94 [1,2]	196 [1,2]	112 [1,2]
22.	16.07.2021	14:30-14:50	100	140	135	-	-	-	132	132	-	-	-
23.	17.07.2021	04:55-05:35	100	-	-	117	-	-	-	-	120 [2];292	-	-
24.	01.08.2021	09:42-09:57	200	211	148	140	-	-	92 [1,2]	66 [1,2]	134 [2]	-	-
25.	01.08.2021	20:00-21:00	600	672	643	-	-	-	306 [1]	296 [1]	-	-	-
26.	20.08.2021	15:40-16:00	200	251	251	251	-	-	108 [1]	104 [1]	102 [1]	-	-
27.	20.08.2021	21:30-22:00	600	567	567	567	-	-	260 [1]	270 [1]	272 [1]	-	-
28.	21.08.2021	22:08-22:35	100	88	83	-	-	-	84	78	-	-	-
29.	24.08.2021	14:20-14:50	400	408	408	-	-	-	216 [1]	218 [1]	-	-	-
30.	26.08.2021	05:20-06:00	600	512	483	483	-	-	250 [1]	244 [1]	276 [1]	-	-
31.	26.08.2021	17:45-18:30	600	596	596	562	-	-	300 [1]	296 [1]	282 [1,2]	-	-
32a.	28.08.2021	05:30-06:45	600	746	720	696	-	-	336 [1]	318 [1]	264 [1]	-	-
32b.	28.08.2021	05:40-06:15	200	-	-	160	160	-	-	-	158;254	170 [2];246	-
33.	29.08.2021	09:50-11:30	1000	1018	987	-	-	-	940 [1]	936	-	-	-
34.	29.08.2021	17:05-17:32	200	-	359	149	-	-	-	266 [1]	150 [2];228	-	-
35.	14.09.2021	01:45-02:35	600	482	350	-	-	-	468	366	-	-	-
36.	14.09.2021	03:20-04:10	200	281	281	-	-	-	146;280	280	-	-	-
37.	14.09.2021	05:10-05:45	200	201	201	-	-	-	196;302	196	-	-	-
38.	14.09.2021	09:10-09:30	200	153	153	-	-	-	154	160	-	-	-
39.	15.09.2021	04:00-04:30	200	324	314	314	-	-	176;322	152;312	150;300	-	-
40.	23.09.2021	04:18-04:40	200	563	563	492	-	-	216 [1,2]	216 [1,2]	198 [1,2]	-	-
41.	29.09.2021	21:45-22:00	100	157	96	-	-	-	146 [2]	44;94 [2]	-	-	-
42a.	09.10.2021	06:22-06:52	200	-	-	186;222	128.48;186.05	186.05;261.33	-	-	112;198 [2],	122;194	118
42b.	09.10.2021	06:22-06:52	100	-	-	57;126	59;126	-	-	-	58 [2];114	60;124 [2]	-
43.	12.10.2021	01:40-01:50	100	75	75	-	-	-	72	38;72	-	-	-
44.	12.10.2021	15:55-16:10	60	69	-	-	-	-	34 [2];74 [2]	-	-	-	-

Notes. Symbols:
[(1)] maximum of the Lomb-Scargle periodogram outside the range of the autocorrelation method
[(2)] maximum on the border of the significance level

Table A.1. Continued.

No.	Date	Duration of pulsations	Smoothing window width [s]	Period of Lomb-Scargle preiodogram [s]					Period of autocorrelation method [s]				
				4-10 keV	10-15 keV	15-25 keV	25-50 keV	50-84 keV	4-10 keV	10-15 keV	15-25 keV	25-50 keV	50-84 keV
45.	21.10.2021	08:00-08:30	200	199	199	-	-	-	98;186	102;190 [2]	-	-	-
46.	25.10.2021	21:50-22:20	200	222	222	175	-	-	100;204 [2]	100;192 [2]	96;185 [2]	-	-
47.	27.10.2021	05:15-06:40	600	733	733	733	-	-	324;762	326;762	340;768	-	-
48.	27.10.2021	18:45-19:40	100	692	692	-	-	-	332 [1]	310 [1]	-	-	-
49.	01.11.2021	01:22-01:40	64	-	55;84	84	-	-	-	80	86	-	-
50.	02.11.2021	02:22-02:50	100	-	-	115;220	-	-	-	-	112	-	-
51.	09.11.2021	15:55-17:00	600	-	-	436	-	-	-	-	430	-	-
52.	04.12.2021	07:00-08:00	600	436	436	-	-	-	210;442	412	-	-	-
53.	04.12.2021	08:20-08:35	200	148	140	-	-	-	144	134	-	-	-
54.	14.12.2021	16:35-17:00	200	230	230	-	-	-	120;228	112;221	-	-	-
55.	18.12.2021	17:30-18:30	600	463;868	478;820	297;820	-	-	452 [1]	456 [1]	454 [1]	-	-
56.	20.12.2021	11:15-11:50	600	-	-	332	-	-	-	-	330	-	-
57.	20.12.2021	20:00-22:30	1000	686	686	656	-	-	662	662	656	-	-
58.	21.12.2021	22:30-23:00	600	475	475	408	-	-	224 [1]	216 [1]	184 [1]	-	-
59.	25.12.2021	13:20-13:35	100	230	157	194	-	-	90 [1,2]	146 [1,2]	94 [1,2]	-	-
60.	01.01.2022	07:10-07:50	600	676	676	676	-	-	322 [1]	320 [1]	302 [1]	-	-
61.	14.01.2022	13:05-13:40	320	-	433	317	-	-	-	208 [1,2]	178 [2];308 [2]	-	-
62.	18.01.2022	17:15-17:50	400	-	-	422;221	-	-	-	-	214 [1]	-	-
63.	29.01.2022	09:00-09:20	100	195	195	-	-	-	104 [1,2]	88 [1,2]	-	-	-
64.	29.01.2022	12:00-12:25	160	-	298	232	-	-	-	158 [1]	128 [1]	-	-
65.	29.01.2022	19:50-20:30	240	360	232	-	-	-	330	344 [2]	-	-	-
66.	29.01.2022	22:30-23:30	400	-	-	400	-	-	-	-	336 [2]	-	-
67.	01.02.2022	03:30-04:30	400	-	362	-	-	-	-	364 [2];522	-	-	-
68.	01.02.2022	09:45-10:45	400	464	464	-	-	-	224 [1]	202 [1]	-	-	-
69.	01.02.2022	22:25-22:40	200	-	283;168	157	-	-	-	86 [2];146 [2]	146	-	-
70.	03.02.2022	07:20-07:45	240	287	230	242	-	-	146 [1]	150;231 [2]	236	-	-
71.	04.02.2022	02:00-03:16	1000	720	746	-	-	-	362;704 [2]	356;735 [2]	-	-	-
72.	09.02.2022	18:45-20:15	200	873	417;873	-	-	-	466;849	458;881	-	-	-
73.	13.02.2022	01:40-02:00	200	392	392	220	-	-	162 [1]	154 [1]	100 [1]	-	-
74.	28.02.2022	09:00-09:30	400	319	319	302	-	-	162 [1]	158 [1]	154 [1]	-	-
75.	02.03.2022	16:55-17:10	60	86	83 [2]	86 [2]	-	-	126;86	82	80 [2]	-	-
76.	02.03.2022	17:15-18:30	400	632	613	-	-	-	318;560 [2]	302;554 [2]	-	-	-
77.	02.03.2022	19:20-19:40	240	167	160	153	-	-	79;178 [2]	76;158 [2]	72;144 [2]	-	-
78.	04.03.2022	00:20-01:00	400	457	457	269	-	-	192 [1]	236 [1,2]	236 [2]	-	-
79.	04.03.2022	04:30-05:10	400	308	297	-	-	-	328	294	-	-	-
80.	05.03.2022	19:30-20:45	600	575	582	517	-	-	545;1180	548;1186	536	-	-
81.	06.03.2022	09:45-10:47	600	672	672	-	-	-	616 [1]	616 [1]	-	-	-
82.	14.03.2022	02:20-02:40	200	220	220	207	-	-	116 [1]	120 [1]	124 [1]	-	-
83.	15.03.2022	22:30-23:59	600	752	752	475;752	-	-	736	734	738	-	-
84.	20.03.2022	07:30-07:40	200	-	-	157	-	-	-	-	144 [2]	-	-
85.	23.03.2022	01:20-01:40	160	160	176	-	-	-	78	72	-	-	-
86.	24.03.2022	06:45-07:50	400	297	297	302	-	-	290	296	296	-	-
87.	24.03.2022	11:00-11:30	400	475	439	-	-	-	238 [1]	222 [1]	-	-	-
88.	25.03.2022	05:00-05:30	240	-	-	230	-	-	-	-	230	-	-
89.	25.03.2022	17:20-17:40	240	352	352	-	-	-	170 [1]	162 [1]	-	-	-
90.	27.03.2022	21:50-22:50	600	510	510	-	-	-	266;492	268;510	-	-	-
91a.	28.03.2022	00:50-05:00	1000	943	949	821	-	-	442;970	966	1968 [2];971 [2]	-	-
91b.	28.03.2022	01:20-02:25	1000	913	913	913	-	-	420 [1]	552 [1]	418 [1]	-	-

Notes. Symbols:
[(1)]maximum of the Lomb-Scargle periodogram outside the range of the autocorrelation method
[(2)]maximum on the border of the significance level